Research Paper

Assessment of thermal modeling of photovoltaic panels for predicting power generation using only manufacturer data

Sara Pereira [a,*], Paulo Canhoto [a,b], Takashi Oozeki [c], Rui Salgado [a,d]

[a] *Institute of Earth Sciences, University of Évora, Rua Romão Ramalho 59, Évora 7000-671, Portugal*
[b] *Department of Mechatronics Engineering, University of Évora, Rua Romão Ramalho 59, Évora 7000-671, Portugal*
[c] *Renewable Energy Research Center, National Institute of Advanced Industrial Science and Technology, 2-2-9 Machiikedai, Koriyama, Fukushima 963-0298, Japan*
[d] *Physics Department, University of Évora, Rua Romão Ramalho 59, Évora 7000-671, Portugal*

A B S T R A C T

This study presents an assessment of thermal modeling for photovoltaic modules, focusing on power output prediction using manufacturer-provided data along with irradiance and weather-related variables. Several steady-state thermal models based on empirical correlations were evaluated for computing the temperature of the photovoltaic module. Additionally, a dynamic model was developed based on the energy conservation equation, incorporating the effects of wind speed and direction, using only manufacturer data and other parameters available in the literature. The performance of these models was evaluated against measured temperatures on the backsides of photovoltaic modules. The models were further integrated with the simple estimate with temperature correction and single diode and five-parameter electrical models to assess combined power output prediction performance. Results show that the Mattei steady-state model is the most accurate for temperature estimation, with a mean bias error of $-0.4°C$ and a root mean squared error of $2.7°C$. For power output estimation, the Kurtz (Sandia1) model combined with the simple estimate with temperature correction outperforms others, showing a mean bias error of 4.6 W and a root mean squared error of 54.5 W. This study systematically evaluates and compares the performance of thermal models for different photovoltaic systems, offering a framework for selecting appropriate models based on their accuracy in temperature estimation and power output prediction. These models can support operational photovoltaic forecasts without the need for production data and facilitate decision-making in the deployment and management of photovoltaic technology.

1. Introduction

A photovoltaic module is a device that converts sunlight into electrical energy through the photovoltaic effect occurring in a junction of two dissimilar semiconductor materials. The generated electricity can vary rapidly due to the variability of the solar resource. Solar irradiance is affected by factors such as the presence of clouds and aerosols in the atmosphere. Moreover, photovoltaic power output is also very impacted by temperature since higher values of module temperature result in a decrease in conversion efficiency (Kalogirou, 2009). Previous studies have extensively explored the impact of environmental parameters such as irradiation, temperature, and dust on the performance of PV systems, leading to the development of various empirical correlation forms to enhance the accuracy of PV modeling. All these aspects are important because, with the increase in installed capacity of photovoltaic systems

throughout the world, the need for modelling such a variable electricity generation has also increased. Accurate models of the conversion from sunlight into electricity can allow for better planning and development of photovoltaic power plants, monitoring system performance, and can also be included in electricity generation forecasting for better control of the electric grid.

Many electrical models of photovoltaic cells have been developed in the literature. Among these models, the level of detail, and therefore the number of input parameters, may vary widely (Gholami et al., 2022a), ranging from simple models where the electrical power produced is assumed to be proportional to solar irradiance, to very detailed models such as the equivalent electric circuit models (Castro, 2018; Evans and Florschuetz, 1977). The most widely used models are single diode models, typically involving three to five parameters for optimal performance analysis. The parameter extraction is a key issue due to the number of parameters to determine and the nonlinearity of the

---

* Corresponding author.
E-mail address: spereira@uevora.pt (S. Pereira).

Nomenclature

A	Area of the photovoltaic module (m^2)
A_s	Photovoltaic module azimuth (°)
C_{mod}	Heat capacity of the module (J/K)
c_{p,T_f}	Specific heat capacity of air film at temperature T_f (J/Kg/K)
DHI	Direct horizontal irradiance (W/m^2)
DIF	Diffuse horizontal irradiance (W/m^2)
DNI	Direct normal irradiance (W/m^2)
g	Gravitational Acceleration (9.8 m/s^2)
Gr	Grashof number
GTI	Global tilted irradiance (W/m^2)
h	Convective heat transfer coefficient (W/m^2/K)
h_{rad}	Radiative heat transfer coefficient (W/m^2/K)
I_0	Reverse saturation current (A)
IAM	Incidence angle modifier
I	Electric current (A)
I_{mp}	Current at maximum power point (A)
I_{pv}	Photovoltaic current (A)
I_{sc}	Short-circuit current (A)
K	Boltzman constant (1.38×10^{-23} J/K)
K_g	Extinction coefficient of the glazing (m^{-1})
k_{T_f}	Thermal conductivity of air film at temperature T_f (W/m/K)
L	Length of the module (m)
L_c	Characteristic length of the module (m)
L_{free}	Length of the module along the natural convection air flow (m)
L_g	Glazing thickness (m)
m	Diode ideality factor
n	Refractive index
N_s	Number of photovoltaic cells in series
Nu	Nusselt number
P	Power output (W)
P_e	Estimated power output (W)
P_{max}	Maximum power output (W)
Pr	Prandtl number
q	Electrical charge of the electron (1.6×10^{-19} C)
Q_{cond}	Net rate of energy loss to the environment by conduction (W)
Q_{conv}	Net rate of energy loss to the environment by convection (W)
Q_{rad}	Net rate of energy loss to the environment by radiation (W)
Q_{sun}	Net in-plane solar irradiance (W)
Re	Reynolds number
Ra	Rayleigh number
R_p	Parallel or shunt resistance (Ω)
R_s	Series resistance (Ω)
S	Incident irradiance (W/m^2)
T	Temperature (°C)

T_a	Air temperature (°C)
T_f	Temperature of air film at the surface of the module (°C)
T_{ground}	Temperature of the ground surface (°C)
T_{mod}	Mean temperature of the photovoltaic module (°C)
T_{sky}	Apparent sky temperature (°C)
U_{pv}	Coefficient of thermal losses from Mattei model (W/°C/m^2)
V	Voltage (V)
V_{mp}	Voltage at maximum power point (V)
V_{oc}	Open-circuit voltage (V)
V_T	Thermal voltage (V)
W	Width of the module (m)
WD	Wind direction (North is assumed 0°) (°)
WD_s	Wind direction (South is assumed 0°) (°)
WS	Wind speed (m/s)
x_{cr}	Critical length (m)

Greek symbols

$\alpha_{I_{sc}}$	Thermal coefficient of short-circuit current (%/°C)
$\alpha_{P_{max}}$	Thermal coefficient of maximum power (%/°C)
$\alpha_{V_{oc}}$	Thermal coefficient of open-circuit voltage (%/°C)
α_{T_f}	Thermal diffusivity of air film at temperature T_f (m^2/s)
β	Tilt angle (°)
ε	Silicon bandgap ($= 1.12$ eV)
ε_b	Emissivity of the back surface of the module
ε_f	Emissivity of the front surface of the module
η	Photovoltaic module efficiency
θ	Angle of incidence (°)
θ_r	Angle of refraction (°)
ν_{T_f}	Kinematic viscosity of air (m^2/s)
σ_{SB}	Stefan-Boltzmann constant (5.670×10^{-8} W/m^2/K^4)
τ	Transmittance

Acronyms and Abbreviations

1d3p	Single diode and 3 parameters model
1d4p	Single diode and 4 parameters model
1d4p$_m$	Single diode and 4 parameters model with ideality factor adjustment
1d5p	Single diode and 5 parameters model
GPI	Global performance index
HIT	Heterojunction intrinsic thin layer
IEC	International electrotechnical commission
MBE	Mean bias error
rMBE	Relative mean bias error
RMSE	Root mean squared error
R^2	Coefficient of determination
rRMSE	Relative root mean squared error
SE	Simple estimate model
SET	Simple estimate with temperature correction model
STC	Standard test conditions

optimization problem, usually requiring numerical or analytical methods and curve fitting methods (Abbassi et al., 2018). Precisely adapting the parameters to real conditions is essential for accurate power output estimates. For the crystalline silicon technology, the five parameter single diode model shows a good balance between accuracy and computation time (Gholami et al., 2022a), although additional adaptations are needed for other technologies such as microcrystalline, amorphous, and cadmium telluride (Mermoud and Lejeune, 2010). Numerous studies review and compare different electric models, presenting advantages and disadvantages derived from simulation or

experimental tests (Castro, 2018; Chenni et al., 2007; Chin et al., 2015; Fahim et al., 2022; Gholami et al., 2022a; Hasan and Parida, 2016; Ma et al., 2014; Roberts et al., 2017). These analyses emphasize the importance of accurately capturing the electrical behavior of photovoltaic modules for reliable power output estimation.

When the temperature of photovoltaic cells/modules is not available, a thermal model is also needed for accurate power output estimation. Most thermal models used in the literature are steady-state and empirical, often biased towards specific technologies, material properties or locations. (Tuomiranta et al., 2014) obtained different correlations

between module temperature (seven different semiconductor materials) and solar irradiance, air temperature and wind speed for Abu Dhabi. (Coskun et al., 2017) tested seventeen different correlations available in the literature for a photovoltaic powerplant in Turkey, modifying them for a better fit to the experimental data. The modified Chenni correlation (Coskun et al., 2017) was shown to be the most suitable under variable wind speed conditions. A comprehensive list of explicit and implicit correlations for module temperature estimation found in the literature is available in (Skoplaki and Palyvos, 2009). Most models typically incorporate solar irradiance, air temperature and wind speed, while additional parameters such as air humidity and dust deposition can also impact photovoltaic system performance. (Gholami et al., 2023) investigated the effect of these variables on photovoltaic panel temperature, finding standardized Beta coefficients of 0.541, 0.645, −0.035, −0.055, and −0.068 for irradiation, ambient temperature, humidity, wind speed, and dust accumulation, respectively. Their proposed semi-empirical correlations achieved coefficients of determination ranging from 0.728 to 0.974. Additionally, studies have shown that dust accumulation impacts the performance of photovoltaic systems, causing both reduced power generation and increased module temperatures (Gholami et al., 2022b; Kazem et al., 2022).

Physical models based on the energy conservation equation for dynamic regimes and heat transfer modeling can reproduce the thermal response of photovoltaic modules over time under variable conditions, making them suitable for simulations with smaller timesteps, typically at a second or minute time scale. Most studies in the literature consider either the electrical or the thermal model alone, or when both are considered, they are often uncoupled (Gholami et al., 2022a). Since the photovoltaic cell/module temperature depends on the electrical power generated and vice-versa, coupling thermal and electrical models is advantageous. Some of the few works that include this coupling were developed recently (Li and Wu, 2022; Perovic et al., 2019). (Perovic et al., 2019) developed a dynamic model that includes the dependence of electric power on module efficiency and temperature, comparing temperature results with measurements in three different points on the back of a photovoltaic module. (Li and Wu, 2022) developed a 3-D thermal model which, when coupled with the single diode 5 parameters electric model, resulted in values of power output, back-surface temperature, and current-voltage curves consistent with observations. In (Torres-Lobera and Valkealahti, 2014), a model for module temperature and power output estimation incorporating a dynamic thermal model and the single diode 5 parameter model, considering parasitic effects and bypass diodes, as well as site-specific adjusting parameters, was developed. In this case, root mean square error of $1.34°C$ for module temperatures and a normalized root mean square error of 1.98 % for power-voltage curves were found. (Gu et al., 2019) assessed thermal resistance distribution and environmental effects on photovoltaic module performance through a coupled electrical-thermal model, highlighting the significance of radiative and convective thermal resistances. In (Tina, 2010), coupled electrical and thermal models for photovoltaic module temperature estimation was presented using inputs such as electric voltage and current, ambient temperature, wind speed and direction, total irradiance, and relative humidity. (Bevilacqua et al., 2021) developed and validated a one-dimensional thermal model for photovoltaic modules, using the energy balance of individual layers in dynamic conditions and determining the temperature distribution across the module cross-section through a finite difference method. In (Tuncel et al., 2020) a dynamic coupled thermal-electric model considering irradiance, air temperature, wind speed and direction, module parameters and geospatial data was developed for hourly data and assessed against observations of a poly-crystalline photovoltaic module, resulting in an MBE of 3.35 W/m^2.

This work systematically evaluates and compares thermal models for different photovoltaic systems, focusing on the accuracy of temperature estimation and power output prediction. It focuses on models that take only as inputs the characteristic values commonly provided by manufacturers in the datasheets, beside solar irradiance and meteorological variables. Data-based models such as regression or machine learning models were not included in the analysis. Experimental values of environmental variables and power output of a photovoltaic system are used for model assessment. Additionally, a developed electric-thermal coupled model for dynamic regimes, considering the wind direction relative to module rows, is also included in the analysis and validated against the same data. All models are compared to find the most accurate method for estimating power output of photovoltaic systems without needing measurements from the system. The novelty of this work lies in several key aspects. Firstly, a transient thermal model was developed that extends beyond traditional steady-state models, enabling predictions under varying operational scenarios. Secondly, a thorough comparative analysis of multiple thermal models was conducted, evaluating their performance against measured data from several PV technologies. This comprehensive evaluation framework ensures robustness of the proposed methodology and strengthens the practical implications for operational decision-making in PV systems. Ultimately, the approach used supports PV forecasts even in the absence of energy generation data, thereby advancing the field's capability for accurate and reliable performance estimation.

This paper is organized as follows: Section 2 presents the methodology of this work specifically the experimental data used for model assessment, including the environmental conditions (solar irradiance, air temperature and wind speed and direction) and photovoltaic system characteristics and power generation data. The various steady-state thermal models of the photovoltaic modules for obtaining module temperature are assessed, and the developed dynamic thermal model is presented. These models are then coupled with the simple estimate with temperature correction and single diode five parameter electric models and validated against observations in Section 3. Finally, Section 4 presents the conclusions of this work.

2. Methodology

The methodology encompasses two main components: data collection and processing, and thermal and electric modeling. Data collection involved retrieving and processing solar resource and meteorological variables, as well as photovoltaic system data. Thermal modeling utilized both steady-state and dynamic models to estimate module temperatures under changing environmental conditions. Coupling the thermal with electric models allows for the estimation of photovoltaic power output. The chapter discusses the formulation of empirical and physics-based models and the rationale behind model selection.

2.1. Data

Data from four different photovoltaic systems located at Fukushima Renewable Energy Institute (FREA, AIST), Koriyama, Japan (37.4495° N, 140.3144° E, Fig. 1) were utilized in this study. The systems employ different photovoltaic cell technologies: one with polycrystalline modules, two with monocrystalline modules, and one using heterojunction technology with intrinsic thin layer (HIT), which combines monocrystalline and amorphous silicon with dissimilar band gaps. The characteristics of these systems are presented in Table 1.

The experimental data comprise environmental variables and photovoltaic system variables. Environmental variables include global tilted solar irradiance (GTI) measured using a class A pyranometer (Hukseflux CHF-SR20-JM), direct normal irradiance (DNI) measured using a pyrheliometer, air temperature (T_a), wind speed (WS) and wind direction (WD) at 7.4 m height. Photovoltaic system variables comprise power output (P) and temperature at the back of the module (T_{mod}), measured with a type T thermocouple attached with Kapton tape directly to the back of one module per system. These variables were recorded at 1-minute timestep and converted to 10-minute mean values. The dataset spans from January 1st 2017 to December 31st 2020. Data
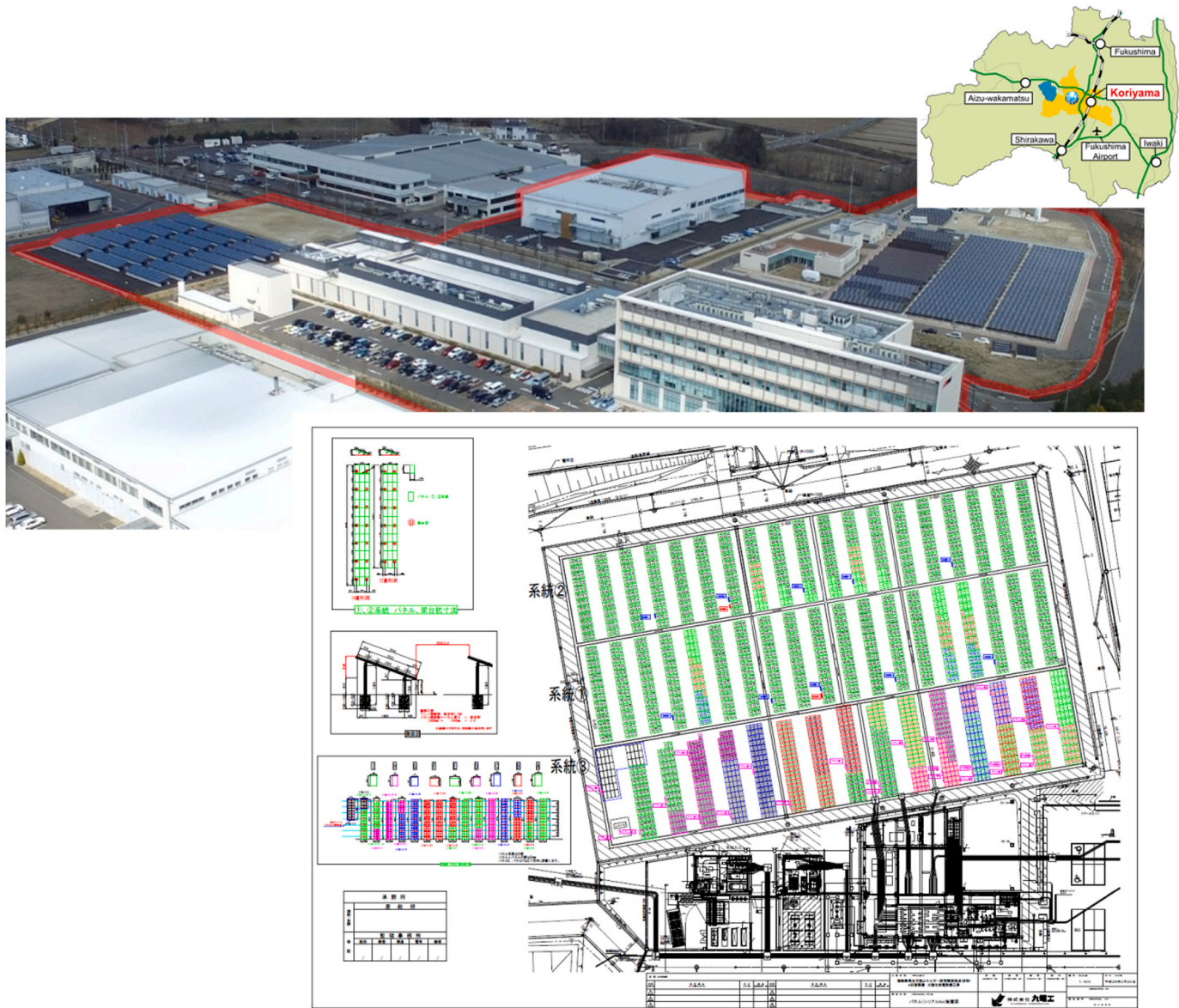
Fig. 1. Location and plan of the photovoltaic systems at FREA, AIST.

preprocessing excluded winter months (December through March) due to snow accumulation on modules, retaining records with valid values across all variables. This resulted in a total of 24543 10-minute data points per system during the daylight hours.

2.2. Thermal modeling of photovoltaic modules

When the measured temperature of the modules is unavailable, a model for its estimation is necessary. Specifically, a model that can accurately estimate the temperature using easily available meteorological variables and characteristics of the photovoltaic systems is required. From the models described in the literature, two main categories can be found: steady-state and dynamic models.

Steady-state models are most common and assume that the heat transfer rate between the modules and the environment is quasi-stationary. In contrast, dynamic models consider the variation in thermal energy storage in the module and heat transfer rates over time. Steady-state models are usually correlations based on experimental data, which can make these models biased towards specific climates or technologies. Dynamic models tend to be based on physical principles

and are more suitable for estimations made over small timesteps.

2.2.1. Steady state models

The steady-state models analyzed in this work are amongst the most commonly used thermal models in the literature and typically require air temperature (T_a), global tilted irradiance (*GTI*) and wind speed (*WS*).

2.2.2. Modified Chenni thermal model

The Chenni thermal model (Chenni et al., 2007) was improved by examining the trend in the temperature difference between the model's results and observation data, resulting in the modified Chenni thermal model (Coskun et al., 2017), as shown in Eq. (1). The observation data used results from a year of records from a polycrystalline powerplant in Turkey.

$$\begin{aligned} T_{\mathrm{mod}} = & T_a - 1.93666 + 0.0138 GTI(1 + 0.031 \quad T_a)(1 - 0.042WS) \\ & + 0.007882 GTI - 0.0000134647(GTI)^2 \end{aligned} \quad (1)$$

2.2.3. Mattei thermal model

The Mattei thermal model (Mattei et al., 2006) was developed using

Table 1
Characteristics of the photovoltaic systems for Standard Test Conditions (STC).

System	1	2	3	4
Photovoltaic modules				
Manufacturer	Toshiba	Panasonic	Kyocera	Sharp
Model	TA60M250WA	VBHN238SJ23A	KS242P−3CF3CE	NQ−198AC
Technology	Monocrystalline	HIT	Polycrystalline	Monocrystalline
P_{max} [W]	250.0	238.1	242.0	198.0
V_{mp} [V]	30.96	43.4	29.8	22.4
I_{mp} [A]	8.07	5.50	8.13	8.84
V_{oc} [V]	37.92	52.20	36.90	27.50
I_{sc} [A]	8.62	5.85	8.80	9.50
$\alpha_{P_{max}}$ [%/K]	−0.440	−0.290	−0.450	−0.392
$\alpha_{V_{oc}}$ [%/K]	−0.300	−0.288	−0.320	−0.357
L [m]	1.650	1.580	1.662	1.165
W [m]	0.991	0.812	0.990	0.990
Thickness [mm]	40	35	46	46
Strings				
No. of modules	8	8	8	10
Position	1st row	2nd row	3rd row	5th row
Peak power [W]	2000.0	1904.8	1936.0	1980.0
Inverters				
Manufacturer	Tabuchi Electric	Tabuchi Electric	Tabuchi Electric	Tabuchi Electric
Model	EPU-A-T100P-SB	EPU-A-T100P-SB	EPU-A-T100P-SB	EPU-A-T100P-SB
Efficiency (%)	93	93	93	93
Capacity [kW]	10	10	10	10

observation data from a grid-connected system and a polycrystalline module with eight temperature sensors integrated into the module, resulting in the correlation shown in Eq. (2). The coefficient of thermal losses, U_{pv}, is computed through Eq. (3), and the transmittance and absorption product at a normal incidence angle of irradiance, $(\tau\alpha)_n$, assumes a value of 0.81.

$$T_{\text{mod}} = \frac{U_{pv} \quad T_a + GTI((\tau\alpha)_n - \eta_{STC} \quad (1 - \alpha_{P_{max}} \times T_{stc})}{U_{pv} + GTI\alpha_{P_{max}}\eta_{STC}} \tag{2}$$

$$U_{pv} = 26.6 + 2.3WS \tag{3}$$

2.2.4. Sandia thermal model

The Sandia thermal model (Sandia National Laboratories, n.d.), shown in Eq. (4), was developed for different module and mount types through the experimentally determined coefficients a and b, as presented in Table 2.

$$T_{\text{mod}} = T_a + GTIe^{a+bWS} \tag{4}$$

2.2.5. Faiman thermal model

The Faiman thermal model (Faiman, 2008) is computed using the correlation shown in Eq. (5), derived from observations on seven different photovoltaic modules with mono and polycrystalline silicon cells located at Sede Boqer in the Negev Desert. The observations of GTI and T_{mod} were made using a pyranometer on the plane of array and thermocouples attached to the back of the modules using a small bead of quick-drying epoxy putty.

$$T_{\text{mod}} = T_a + \frac{GTI}{25 + 6.84WS} \tag{5}$$

Table 2
Parameters of the Sandia models.

Name	Module Type	Mount	a	b
Kurtz (Sandia1)	Glass/cell/glass	Open rack	−3.47	−0.0594
Sandia2	Glass/cell/glass	Close roof mount	−2.98	−0.0471
Sandia3	Glass/cell/polymer sheet	Open rack	−3.56	−0.0750
Sandia 4	Glass/cell/polymer sheet	Insulated back	−2.81	−0.0455

2.2.6. JIS thermal model

The JIS thermal model presented in Eq. (6), originates from the Japanese Industrial Standard (Japanese Industrial Standard - Japanese Standards Association, 2005) and was determined for two different mount types, resulting in parameters a and b shown in Table 3.

$$T_{\text{mod}} = T_a + \left(\frac{a}{b \quad WS^{0.8} + 1} + 2\right) \frac{GTI}{G_{STC}} - 2 \tag{6}$$

2.2.7. Migan thermal model

The Migan model (Migan, 2013) is computed using the correlation on module temperature, air temperature, global tilted irradiance, and wind speed, as shown in Eq. (7). This equation is derived from several different assumptions regarding a 5-layer module considering conduction and convection losses and disregarding heat losses due to radiation.

$$T_{\text{mod}} = T_a + \frac{0.32GTI}{8.91 + 2WS} \tag{7}$$

2.2.8. Dynamic model

Dynamic thermal models are based on the energy conservation equation derived from the first law of thermodynamics. For a specific photovoltaic module, an energy balance equation for each material layer can be included in the model (Bevilacqua et al., 2021) or, alternatively, a simpler model can be developed by considering the entire module (Perovic et al., 2019). In this work, since the focus is on general models that only uses parameters provided by the manufacturers, the later approach is followed, and thus the module is considered as a block with an average temperature T_{mod}. This approach is a compromise between the need for input data and parameters and computational effort. The energy balance can be defined by Eq. (8), where C_{mod} is the equivalent heat capacity of the module, Q_{sun} is the net rate of in-plane solar irradiance and Q_{cond}, Q_{conv} and Q_{rad} are the net rates of heat transfer to the environment through conduction, convection and thermal radiation, respectively, and P_e is the electric power output generated by the

Table 3
Parameters of the JIS models.

Name	Mount	a	b
JIS1	Frame	46	0.41
JIS2	Roof	50	0.38

photovoltaic cells.

$$C_{\mathrm{mod}}\frac{dT_{\mathrm{mod}}}{dt} = Q_{\mathrm{sun}} - Q_{\mathrm{cond}} - Q_{\mathrm{conv}} - Q_{\mathrm{rad}} - P_e \tag{8}$$

In (Luketa-Hanlin and Stein, 2012; Tuncel et al., 2020), a sensitivity analysis was performed to evaluate the effect of the heat capacity value on the performance of dynamic thermal models. The results showed that varying this value had very little impact on the modeled temperature and power output of the modules when compared to the remaining terms of the equation. As such, the recommended value of 22800 J/K is applied to any photovoltaic system (Luketa-Hanlin and Stein, 2012).

The absorbed solar energy is computed through Eq. (9) requiring the area of the module, A, provided by the manufacturer, and where S is the absorbed irradiance, $(\tau\alpha)_n$ is the optical efficiency for normal incidence, which is obtained through the product of transmissivity by the typical absorptivity value of 0.9 (Sandia National Laboratories, n.d.). For the equations for the computation of S and $(\tau\alpha)_n$, please check Appendix A. Although each module has both active and inactive areas, in this study, the total area of the photovoltaic module is assumed to be the active area, since the ratio of active to total area is typically close to 1.

$$Q_{\mathrm{sun}} = A \times S \times (\tau\alpha)_n \tag{9}$$

The heat transfer by conduction is considered negligible since the contact area between the module and the supporting structure is small. The net rate of heat transfer by convection can be computed through Eq.

$$h_{f/b} = \begin{cases} h_{f/b,free}, & if\ \dfrac{Gr}{\mathrm{Re}_{f/b}^2} > 100 \\[2mm] \sqrt[3]{h_{f,free}^3 + h_{f,forced}^3}, & if\ 0.1 \leq \dfrac{Gr}{\mathrm{Re}_f^2} \leq 100 \\[2mm] \sqrt[3]{h_{b,free}^3 + h_{b,forced}^3}, & if\ 0.1 \leq \dfrac{Gr}{\mathrm{Re}_b^2} \leq 100 \wedge leeward \\[2mm] \sqrt[3]{h_{b,free}^3 - h_{b,forced}^3}, & if\ 0.1 \leq \dfrac{Gr}{\mathrm{Re}_b^2} \leq 100 \wedge windward \\[2mm] h_{f/b,forced}, & if\ \dfrac{Gr}{\mathrm{Re}_{f/b}^2} < 0.1 \end{cases} \tag{11}$$

$$Gr = Ra/\mathrm{Pr} \tag{12}$$

$$Ra = g(1/T_f)(T_{\mathrm{mod}} - T_a)L^3 \big/ (\nu_{T_f}\alpha_{T_f}) \tag{13}$$

$$\mathrm{Pr} = c_{p,T_f}\nu_{T_f} \big/ k_{T_f} \tag{14}$$

$$\mathrm{Re}_{f/b} = WS \times L_{c,f/b} \big/ \nu_{T_f} \tag{15}$$

$$L_c = \begin{cases} W, if\ windward \wedge\ \ [45 < (WD_s - As) < 135 \vee 225 < (WD_s - As) < 315] \\[2mm] L, if\ windward \wedge\ \ [(WD_s - As) \leq 45 \vee 135 \leq (WD_s - As) \leq 225 \vee (WD_s - As) > 315] \\[2mm] \dfrac{4L \times W}{2(L + W)}, if\ leeward \end{cases} \tag{16}$$

(10), where h_f and h_b are the convective heat transfer coefficients at the front and back of the photovoltaic module, respectively.

$$Q_{conv} = A(h_f + h_b)(T_{\mathrm{mod}} - T_a) \tag{10}$$

Convection can be defined as free (or natural) convection, driven by buoyancy due to temperature gradients in the fluid, or forced convection, driven by external forces, or a combination of both depending on the flow conditions. Eqs. (11) through (16) are used to compute the overall convective heat transfer coefficient of each surface (Kaplanis and Kaplani, 2019). In these equations, L_c represents the length of the module along the airflow direction. The thermodynamic and transport properties of dry air, obtained at 1 atm and film temperature T_f, are

The convective heat transfer coefficient for natural convection is computed through Eq. (17), where L_{free} is the length of the module along the natural airflow (Kaplani and Kaplanis, 2014). The Nusselt number, Nu, is computed using the correlations in Eq. (18) presented by Reiter et al. (2015). The first correlation is used for laminar flow, while the second is used for turbulent flow.

$$h_{f/b,free} = \frac{Nu_{f/b} \times k_{T_f}}{L_{free}} \tag{17}$$

$$Nu_{f/b} = \begin{cases} \left(0.825 + 0.387\sqrt[6]{Ra\,sin(\beta)\left(1 + \left(\dfrac{0.492}{\mathrm{Pr}}\right)^{9/16}\right)^{-16/9}}\right)^2, if\ 0.1 < Ra < Ra_{cr} \wedge \mathrm{Pr} > 0.001 \\[4mm] 0.56(Ra_{cr}cos(\theta_r))^{0.25} + 0.13\left(\sqrt[3]{Ra} - \sqrt[3]{Ra_{cr}}\right), if\ Ra \geq Ra_{cr} \wedge \mathrm{Pr} > 0.001 \end{cases} \tag{18}$$

used. The film temperature is computed through the formula $T_f = T_a + 0.25(T_{\mathrm{mod}} - T_a)$ for natural convection (Fujii and Imura, 1972; Kaplani and Kaplanis, 2014; Reiter et al., 2015). This model considers the wind direction, WD_s, in which 0° is for a wind direction from the South (local reference meridian), through the characteristic length L_c computed by Eq. (16) (Kaplani and Kaplanis, 2014), with A_s representing the photovoltaic module azimuth.

in which the critical Rayleigh value is computed using Eq. (19), where θ_v is given by Eq. (20).

$$Ra_{cr} = 10^{8.9 - 0.00178(\theta_v)} \tag{19}$$

$$\theta_v = 90 - \beta \tag{20}$$

In the case of forced convection, the convective heat transfer

coefficients for the front and back surfaces of the module are calculated considering the wind speed and direction, as shown in Eq. (21). The first correlation is used for laminar flow, the second for transition flow, and the third for turbulent flow (Sartori, 2006). The critical Reynolds number (Re$_{cr}$) is 4×10^5, and L_c is computed using Eq. (16), which also depends on the wind direction.

$$h_{forced, \ f/b} = \begin{cases} 3.83 WS^{0.5} L_c^{-0.5}, if \dfrac{x_{cr}}{L_c} \geq 0.95 \\[3mm] 5.74 WS^{0.8} L_c^{-0.2} - 16.46 \Big/ L_c, if 0.05 \leq \dfrac{x_{cr}}{L_c} < 0.95 \\[3mm] 5.74 WS^{0.8} L_c^{-0.2}, if \dfrac{x_{cr}}{L_c} < 0.05 \end{cases} \tag{21}$$

in which the critical value x_{cr} is given by Eq. (22).

$$x_{cr} = \text{Re}_{cr} v_{T_f} \Big/ \text{WS} \tag{22}$$

The net rate of heat transfer with the environment by thermal radiation is computed using Eq. (23). The radiative heat transfer coefficients for the front and back surfaces of the module are computed using Eqs. (24) and (25), respectively. The sky temperature is obtained in Kelvin through the correlation presented in Eq. (26) (Swinbank, 1963), and the ground temperature (T_{ground}) is assumed to be equal to the air temperature. The emissivity coefficients (ε) are assumed to be 0.85 for the front surface and 0.91 for the back surface (Kaplanis and Kaplani, 2019).

$$Q_{rad} = A \left(h_{rad\ f} \left(T_{mod} - T_{sky} \right) + h_{rad\ ,b} \left(T_{mod} - T_{ground} \right) \right) \tag{23}$$

$$\begin{aligned} h_{rad, f} &= \varepsilon_f \sigma_{SB} \left(T_{mod}^2 + T_{sky}^2 \right) \left(T_{mod} + T_{sky} \right) \frac{1 + \cos(\beta)}{2} \\ &+ \varepsilon_f \sigma_{SB} \left(T_{mod}^2 + T_{ground}^2 \right) \\ &\times \left(T_{mod} + T_{ground} \right) \frac{\left(T_{mod} - T_{ground} \right)}{\left(T_{mod} - T_{sky} \right)} \frac{1 - \cos(\beta)}{2} \end{aligned} \tag{24}$$
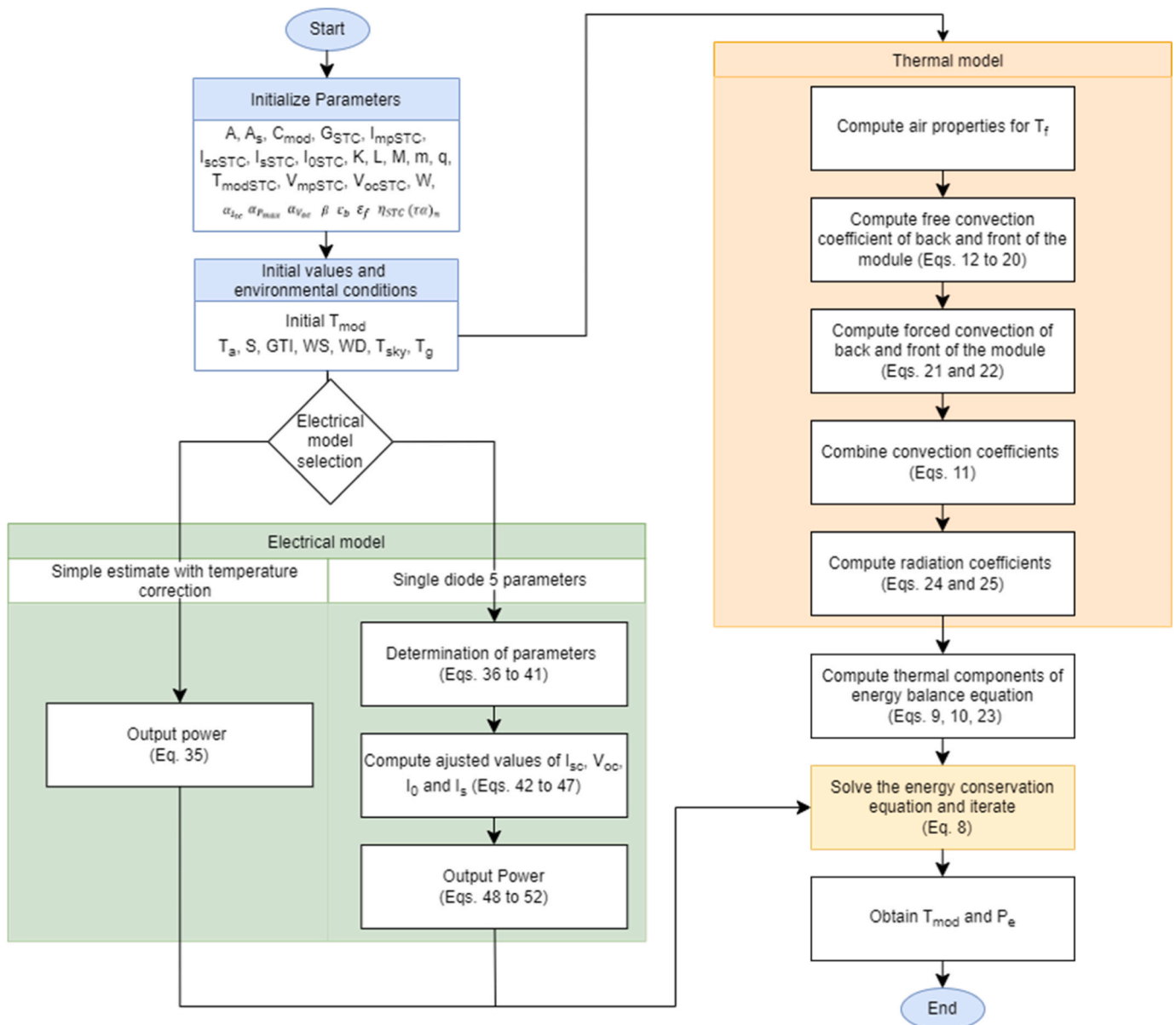
Fig. 2. Dynamic model flowchart.

$$h_{\mathrm{rad},b} = \varepsilon_b \sigma_{SB} \left(T_{\mathrm{mod}}^2 + T_{\mathrm{sky}}^2 \right) \left(T_{\mathrm{mod}} + T_{sky} \right) \frac{\left(T_{\mathrm{mod}} - T_{\mathrm{sky}} \right)}{\left(T_{\mathrm{mod}} - T_{\mathrm{ground}} \right)} \frac{1 + \cos(180 - \beta)}{2}$$
$$+ \varepsilon_b \sigma_{SB} \left(T_{\mathrm{mod}}^2 + T_{\mathrm{ground}}^2 \right) \left(T_{\mathrm{mod}} + T_{\mathrm{ground}} \right) \frac{1 - \cos(180 - \beta)}{2}$$

$$(25)$$

$$T_{\mathrm{sky}} = 0.0552 T_a^{1.5} \tag{26}$$

Finally, the electrical power output of the module, P_e, can be obtained from different models. In this work, the most commonly used electric models–simple estimate with temperature correction, and the single diode and five parameters models (presented in Appendix A)– were coupled to the presented dynamic thermal model. Typical values available in the literature were assumed for different parameters of photovoltaic modules, including surface emissivity (Kaplanis and Kaplani, 2019), glazing transmissivity, module absorptivity (Sandia National Laboratories, n.d.), and heat capacity (Luketa-Hanlin and Stein, 2012). This means the model can be further optimized for improved results by adjusting these parameters.

To solve these equations and simultaneously obtain the module temperature and electrical power output, an iterative method must be applied. In this work, the Dorman and Prince version of the Runge-Kutta formula (Dormand and Prince, 1986) was used through the Matlab function *ode45*.

Fig. 2 illustrates the dynamic model used to estimate the module temperature and electrical power output of photovoltaic systems. This structured approach ensures accurate modeling by integrating thermal and electrical processes.

3. Results and discussion

The thermal models discussed in Section 2 were applied to the study's open rack mounted photovoltaic systems. Models originally designed for roof-mounted or insulated modules, namely Sandia2, Sandia4, and JIS2, were excluded from consideration. The results were assessed against observations as shown in Fig. 3, which presents a direct comparison between estimated module temperature and the measured temperature on the back of the photovoltaic module.

The dynamic thermal model, which incorporates electric power output, was evaluated when coupled with the simple estimate with

Table 4
Statistical indicators of thermal models when compared to the measured temperature.

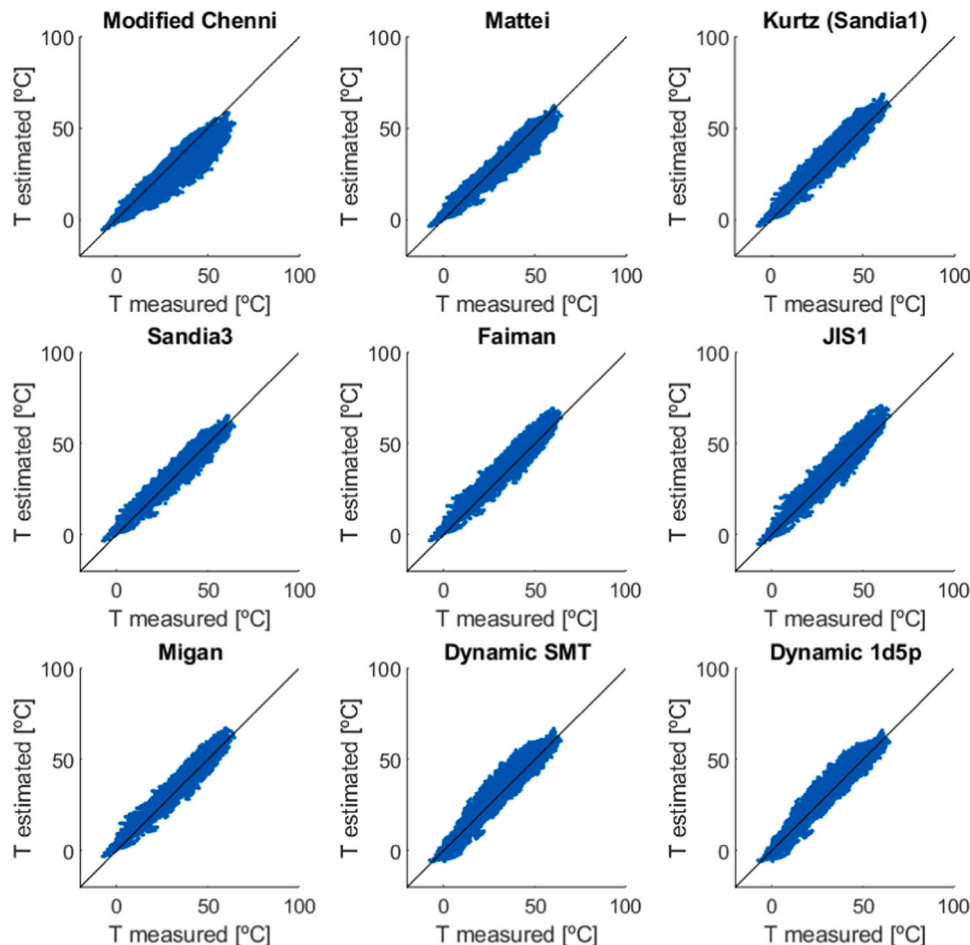| Model	R^2	MBE (°C)	rMBE (%)	RMSE (°C)	rRMSE (%)	GPI
Mattei	0.975	−0.4	−1.8	2.7	13.7	0.620
Sandia3	0.973	0.9	4.6	2.8	14.0	0.328
Migan	0.975	1.2	6.0	2.7	13.6	0.297
JIS1	0.967	0.8	4.0	3.1	15.7	0.072
Faiman	0.969	1.6	8.2	3.0	15.1	−0.159
Dynamic + 1d5p	0.958	−0.4	−2.0	3.6	18.1	−0.205
Dynamic + SET	0.959	−1.0	−5.0	3.6	17.9	−0.395
Kurtz (Sandia1)	0.955	2.0	10.2	3.6	18.3	−0.932
Modified Chenni	0.926	−2.9	−14.4	4.7	23.4	−2.370

Fig. 3. Comparison between measured and estimated temperature with the various models.

temperature correction (SET) and single diode and 5 parameters (1d5p) models. Selection of these electrical models for coupling with the dynamic thermal model was based on preliminary tests demonstrating their suitability and accuracy for predicting the electrical photovoltaic system performance. As detailed in Appendix A, these preliminary evaluations showed that the SET model offers a straightforward yet effective approach for incorporating temperature effects, making it a practical choice for dynamic simulations. On the other hand, the 1d5p model, with its detailed parameterization, provides a more nuanced and precise representation of the electrical characteristics of photovoltaic modules.

The models used in this study are derived from experimental correlations and theoretical assumptions or empirical relations developed by various researchers using data from different technologies and under different environmental conditions. As a result, each model's performance can be affected by the specific characteristics and assumptions inherent in its development. For instance, models differ in how they account for the different heat transfer mechanisms, material properties, and environmental conditions, which leads to variations in their accuracy. While some models, such as the Mattei and Modified Chenni, show negative bias, other overestimate temperatures due to these inherent differences.

This overestimation could also be due to the fact that temperature measurements are taken outside of the photovoltaic module, usually resulting in values slightly lower than the actual photovoltaic cell temperature, which is the output of the thermal models. Detailed results are provided in Table 4, which presents various statistical indicators, namely the correlation coefficient, R^2, mean bias error, MBE, relative mean bias error, rMBE, root mean squared error, RMSE, relative root mean squared error, rRMSE, and a global performance indicator GPI. The GPI allows for the ranking of the models from best to worst (higher to lower value) according to the above metrics (further details can be found in Pereira et al. 2023). Fig. 4 displays a boxplot of these results, providing a visual comparison of the performance of each model relative to others based on MBE, RMSE and GPI metrics.

The assumptions discussed above are confirmed, and the steady-state Mattei model is identified as the best in estimating module temperature, having the highest GPI along with a mean bias error of −0.4 °C and root mean squared error of 2.7 °C. The best dynamic model is shown to be the one coupled with the single diode and 5 parameters electrical model

with a mean bias error of −0.4 °C and root mean squared error of 3.6 °C. In Fig. 4, it is visible that the Modified Chenni and Kurts (Sandia1) models show lower performance, particularly in terms of higher bias and lower accuracy. Detailed results for each model and photovoltaic system can be consulted in Table B.1 in Appendix B.

However, the measured temperature is not the actual mean temperature of the module and, since the goal of this work is to have an accurate estimation of the photovoltaic power output, the thermal models were evaluated in terms of estimated power when coupled with either the simple estimate with temperature correction or the single diode and 5 parameters electrical models. For steady-state models, this involved using the thermal model to estimate module temperature based on environmental conditions such as irradiance and ambient temperature. This estimated temperature is then used in the electrical model to adjust the electrical power output accordingly.

The results for the SET model are presented in Figs. 5 and 6 and Table 5. Here, the estimated and measured electric power are directly compared, with a remarkably similar overestimation for all thermal models. This is also observed when using the measured temperature with the SET model (upper left plot of Fig. 5). The best thermal model (with the highest GPI) coupled with the SET model in terms of power output prediction is shown to be the Kurtz (Sandia1) model with a mean bias error of 4.6 W and root mean squared error of 54.5 W. Using the temperature measured in the back of the module only returns better power estimates when compared with the results for Mattei and Modified Chenni models which show the worst metrics as visible in Fig. 6. The results for each model and photovoltaic system are presented in Table B.2 of Appendix B.

The same analysis was carried out by coupling the thermal models with the single diode and 5 parameters model and the corresponding results can be seen in Figs. 7 and 8 and Table 6.

With this electrical model, an overestimation of the output power is observed for all steady-state thermal models, being the best model the Kurtz (Sandia1) thermal model with a mean bias error of 15.7 W and root mean squared error of 83.6 W. All models, except the Mattei and Modified Chenni models, show better results than the use of measured module temperature when estimating power output with the 1d5p electrical model. The results for each model and photovoltaic system are presented in Table B.3 in Appendix B.

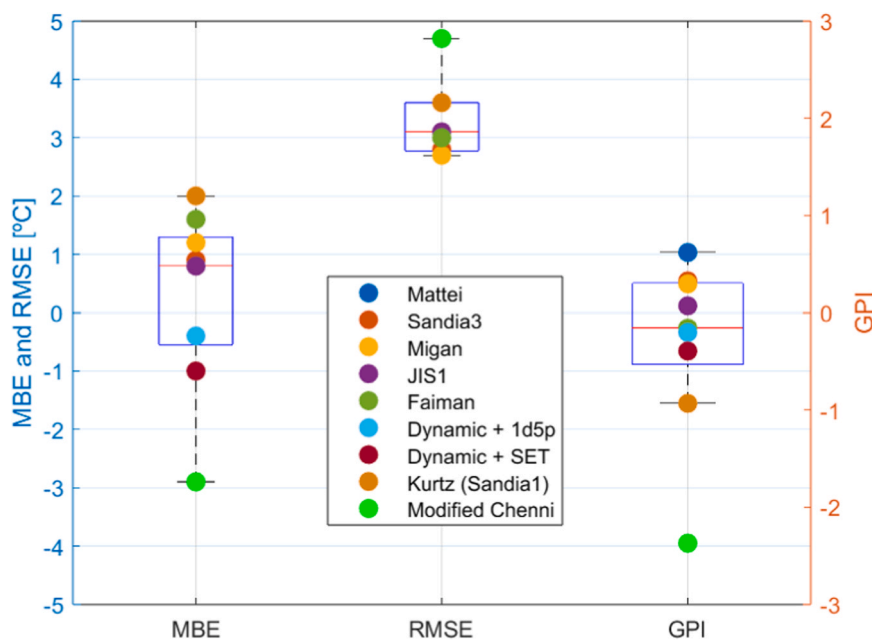Comparing the results shown in Table 5 and Table 6, the best

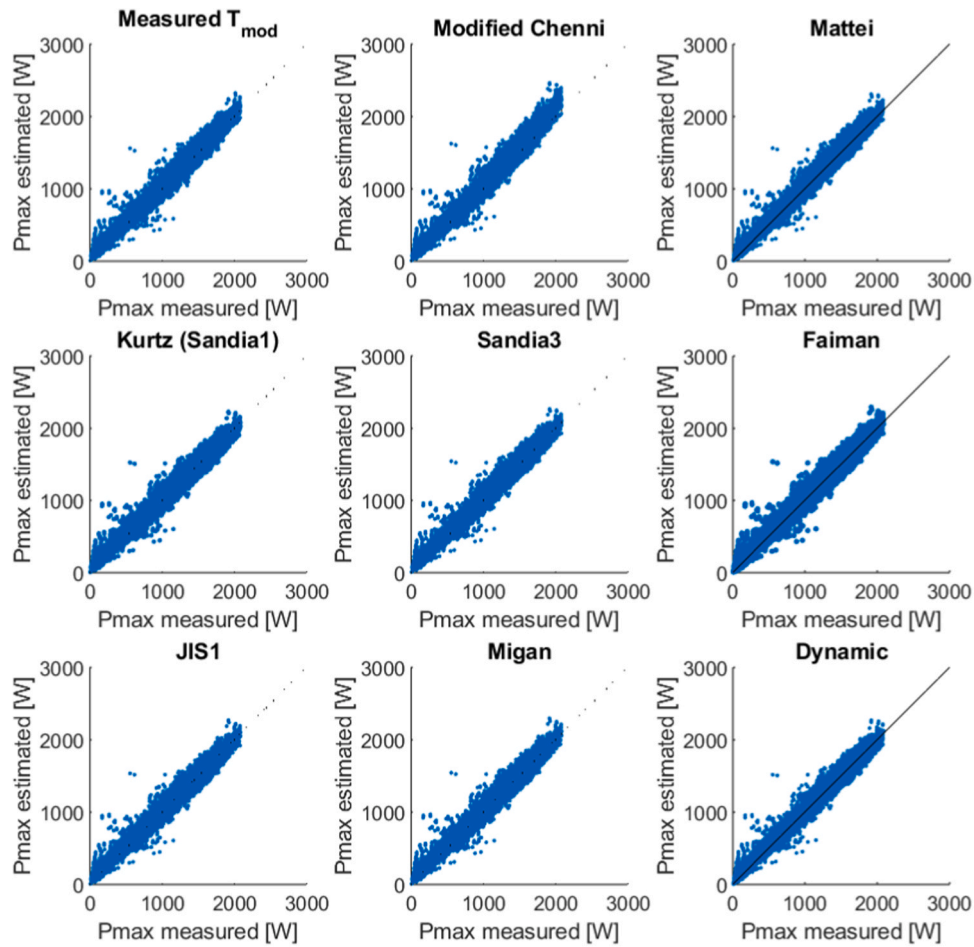**Fig. 4.** Boxplot of thermal model results.

Fig. 5. Comparison between measured and estimated power output with SET model coupled with each thermal model.
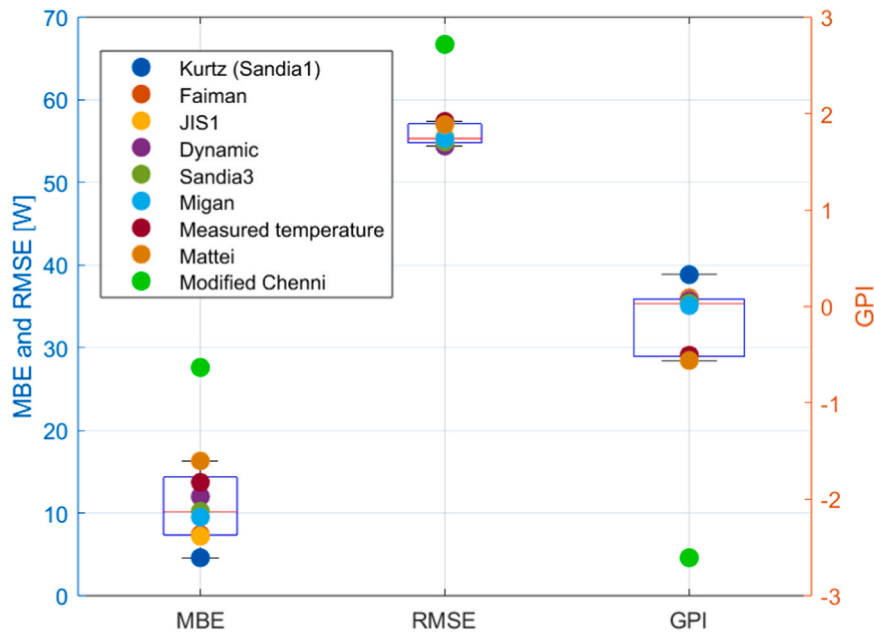
Fig. 6. Boxplot of SET results.

combination of thermal and electrical models for the estimation of power output is shown to be the Kurtz (Sandia1) thermal model with the simple estimate with temperature correction model which shows a mean bias error of 4.6 W and a root mean squared error of 54.5 W. Also, clearly visible when comparing Figs. 6 and 8, the use of the simple estimate with temperature correction model for electric power calculation

Table 5

Statistical indicators of SET model output coupled with each thermal model.

Model	R^2	MBE (W)	rMBE (%)	RMSE (W)	rRMSE (%)	GPI
Kurtz (Sandia1)	0.995	4.6	0.7	54.5	8.5	0.329
Faiman	0.994	7.4	1.2	55.3	8.6	0.088
JIS1	0.994	7.2	1.1	55.5	8.6	0.071
Dynamic	0.995	12.0	1.9	54.4	8.5	0.061
Sandia3	0.994	10.2	1.6	54.9	8.6	0.033
Migan	0.994	9.5	1.5	55.3	8.6	0.008
Measured temperature	0.994	13.7	2.1	57.4	8.9	−0.505
Mattei	0.994	16.3	2.5	57.0	8.9	−0.562
Modified Chenni	0.992	27.6	4.3	66.7	10.4	−2.606

shows greater variability in statistical indicators across different temperature models compared to the single diode 5 parameters model, which has a maximum variation in MBE of 1.5 W between thermal models. This means that when using the 1d5p electrical model, the choice of thermal model is less critical for accurate power output estimation.

While the models considered in this study include the impact of module temperature, irradiance, and some of them wind speed and direction, other meteorological variables such as relative humidity, precipitation in the form of rain or snow, and dust accumulation can also affect the thermal response of photovoltaic modules and deserve further investigation to enhance the robustness of the models.

4. Conclusions

In this work, several thermal models of a photovoltaic module, including a developed dynamic thermal model, were evaluated for their ability to estimate temperature and electrical power output using only the characteristic parameters provided by the module manufacturer. Measurements of GTI and temperature on the back of the module from four different technologies were used for assessment. The best model for estimating the measured temperature was the steady-state Mattei model, achieving an MBE of −0.4 °C. In terms of power output, the Kurtz model coupled with the simple estimate with temperature correction electrical model demonstrated best performance, with an MBE of 4.6 W. When coupled with the single diode and 5 parameter electric model, the MBE was 15.7 W. The single diode 5 parameter model showed consistent results across all thermal models, with a maximum MBE variation of only 1.5 W, indicating the choice of thermal model is less critical when combined with a highly detailed electrical model.

This study provides a comprehensive evaluation of both steady-state and dynamic thermal models, highlighting the importance of selecting appropriate coupling of thermal and electrical models to improve the accuracy of module temperature and power output estimations for photovoltaic systems. It is shown that selecting the most accurate model for estimating module temperature does not necessarily yield the best power output estimates, as the accuracy of power output predictions strongly depends on the selected electrical model. It was also shown that using one of the studied thermal models (excluding the Mattei and Modified Chenni models) results in better estimates of photovoltaic power output than using temperature measurements on the back of the modules.
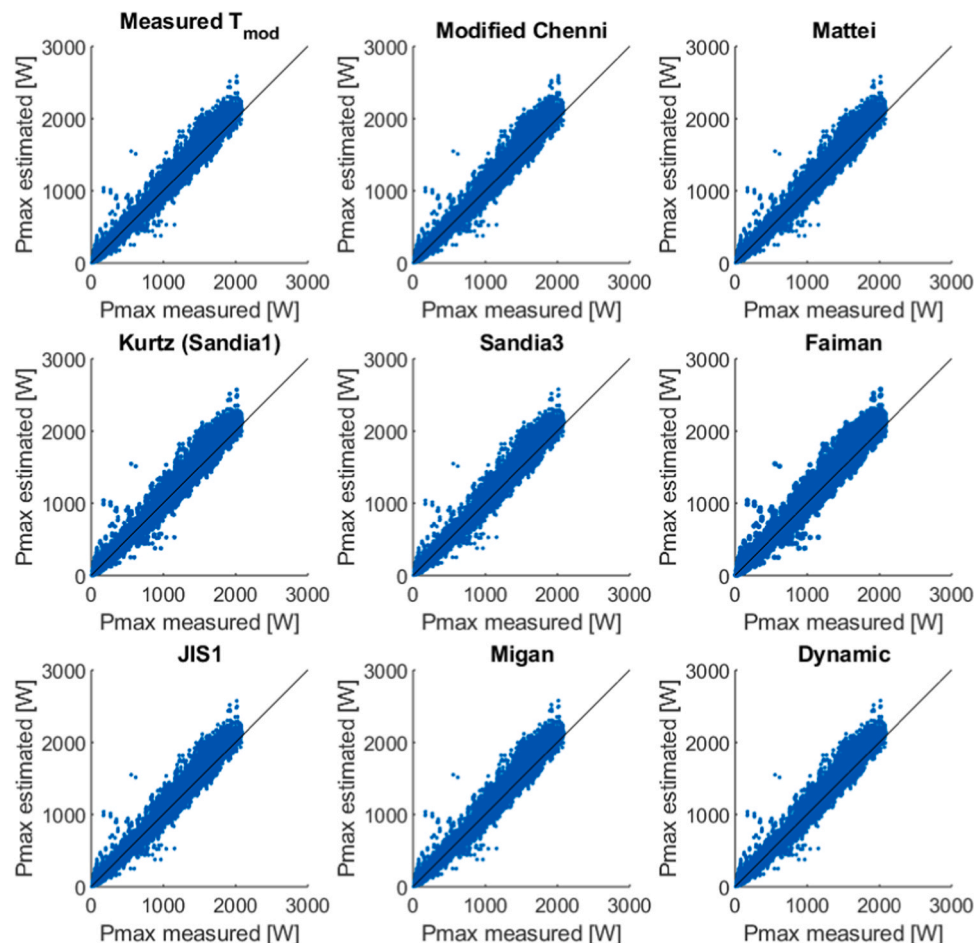

Fig. 7. Comparison between measured and estimated power output with the single diode and 5 parameters model coupled with each thermal model.
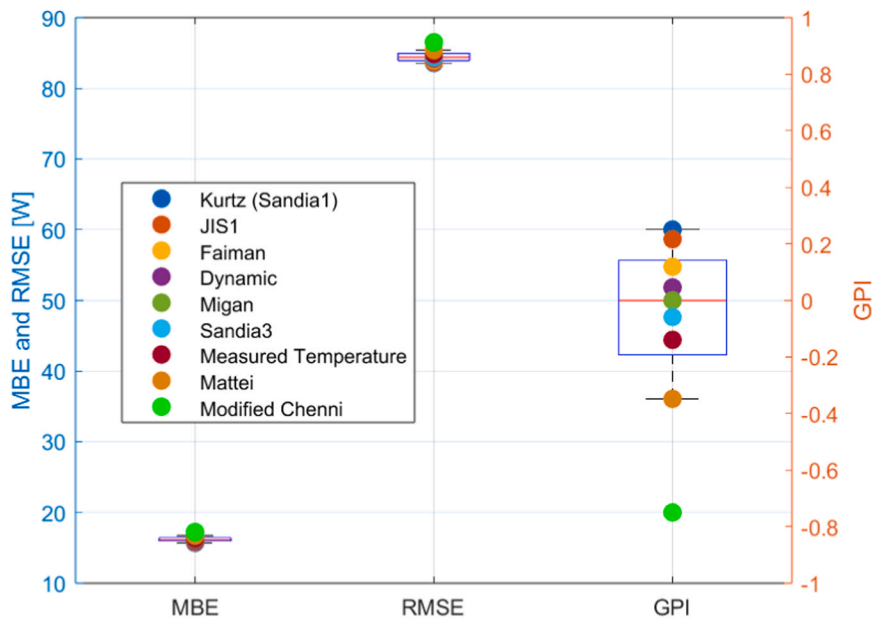
Fig. 8. Boxplot of 1d5p model results.

Table 6
Statistical indicators of single diode and 5 parameters model output coupled with each thermal model.

Model	R^2	MBE (W)	rMBE (%)	RMSE (W)	rRMSE (%)	GPI
Kurtz (Sandia1)	0.987	15.7	2.5	83.6	13.0	0.250
JIS1	0.987	15.8	2.5	83.7	13.0	0.216
Faiman	0.987	16.0	2.5	84.0	13.1	0.119
Dynamic	0.987	16.0	2.5	84.2	13.1	0.046
Migan	0.987	16.2	2.5	84.4	13.1	0.000
Sandia3	0.987	16.3	2.5	84.5	13.2	−0.059
Measured Temperature	0.987	16.3	2.5	84.8	13.2	−0.140
Mattei	0.987	16.7	2.6	85.4	13.3	−0.348
Modified Chenni	0.986	17.2	2.7	86.5	13.5	−0.750

The evaluated models allow researchers and power plant operators to estimate the temperature and power output of PV systems without the need for extensive and costly experimental testing. These models can be employed for forecasting the power output of photovoltaic modules if forecasts of GTI and other relevant weather variables are available. Further refinements in thermal modeling could focus on improving accuracy under varying environmental conditions or specific module technologies, while continuous validation and adaptation of these models with experimental data from power plants could enhance their applicability and reliability in different operational settings.

The findings can aid in the planning and development of PV systems by providing reliable tools for performance estimation, ultimately enhancing the efficiency and feasibility of PV installations. This study highlights the practical benefits and scientific and technological importance of these models, offering valuable insights for optimizing and managing photovoltaic systems, and paving the way for more accurate and efficient renewable energy solutions.

CRediT authorship contribution statement

Rui Salgado: Writing – review & editing, Validation, Supervision, Resources, Project administration, Funding acquisition, Conceptualization. **Sara Pereira:** Writing – original draft, Visualization, Validation, Methodology, Investigation, Formal analysis, Data curation, Conceptualization. **Paulo Canhoto:** Writing – review & editing, Visualization, Validation, Supervision, Software, Resources, Project administration, Methodology, Investigation, Funding acquisition, Formal analysis, Data curation, Conceptualization. **Takashi Oozeki:** Writing – review & editing, Visualization, Validation, Supervision, Software, Resources, Project administration, Methodology, Investigation, Funding acquisition, Formal analysis, Data curation, Conceptualization.

Declaration of Competing Interest

The authors declare that they have no known competing financial interests or personal relationships that could have appeared to influence the work reported in this paper.

Data Availability

The authors do not have permission to share data.

Appendix A. - Electric models of photovoltaic modules

Here, a preliminary review and assessment of standard electric models of photovoltaic modules, namely, a simple estimate model and an equivalent circuit model using a data-driven model as reference, is presented.

The models were evaluated against observations using as input the characteristics of the photovoltaic modules, observed GTI and temperature measured at the back of the modules.

For these models, the incident irradiance, S, is obtained through Eq. (27) (Bevilacqua et al., 2021), where θ_b is the incidence angle of direct solar radiation, θ_d is the equivalent diffuse incidence angle obtained through Eq. (28) (Duffie and Beckman, 2013) which are also used to compute the beam and diffuse incidence angle modifiers, K_{θ_b} and K_{θ_d}, respectively. The incident angle modifier is computed as in Eq. (29) (Duffie and Beckman, 2013). The transmittance values can be obtained through Eqs. (30) and (31), respectively, where θ_r is the angle of refraction computed through Eq. (32). Typical input parameters for photovoltaic modules suggested in (De Soto et al., 2006) were used in this work, namely, the refractive index $n = 1.526$, the extinction coefficient $K_g = 4\ m^{-1}$ and the thickness $L_g = 0.002m$ of the glazing.

$$S = DNI\cos\theta_b K_{\theta_b} + (GTI - DNI\cos\theta_b)K_{\theta_d} \tag{27}$$

$$\theta_d = 59.7 - 0.1388\beta + 0.001497\beta^2 \tag{28}$$

$$K_\theta = \frac{\tau(\theta)}{\tau(0)} \tag{29}$$

$$\tau(\theta) = e^{-\left(\frac{K_g L_g}{\cos(\theta_r)}\right)} \left[1 - \frac{1}{2}\left(\frac{\sin^2(\theta_r - \theta\ \ )}{\sin^2(\theta_r + \theta\ \ )} + \frac{\tan^2(\theta_r - \theta\ \ )}{\tan^2(\theta_r + \theta\ \ )}\right)\right] \tag{30}$$

$$\tau(0) = e^{-\left(K_g L_g\right)}\left[1 - \left(\frac{1-n}{1+n}\right)^2\right] \tag{31}$$

$$\theta_r = \sin^{-1}\left[\frac{1}{n}\sin(\theta)\right] \tag{32}$$

where β stands for the tilt angle of the modules. The air mass modifier is computed as in Eqs. (33) and (34) (Duffie and Beckman, 2013), where the constants denoted as a_i can be obtained from (De Soto et al., 2006) for different photovoltaic cells. In this case, the coefficients for monocrystalline silicon were employed, since De Soto et al. (De Soto et al., 2006) also showed that selecting a single set of coefficients and applying them for any cell type results in outcomes which are comparable to using different air mass modifier relationships for each cell type.

$$M = \sum_0^4 a_i(AM)^i \tag{33}$$

$$AM = \frac{1}{\cos(\theta_z) + 0.5057(96.080 - \theta_z)^{-1.634}} \tag{34}$$

The simple estimate model with temperature correction (SET) (Evans and Florschuetz, 1977) is described by Eq. (35), where the estimated power output is directly proportional to the solar irradiance absorbed by the photovoltaic module (S) and the air mass modifier (M) as well as to some characteristics of the modules, namely its efficiency at STC given by the manufacturer (η_{STC}) and the surface area (A), including a correction due to the module temperature as in (Evans and Florschuetz, 1977).

$$P_e = \eta_{STC} \times A \times S \times M \times \left(1 + \alpha_{P_{max}} \times (T_{mod} - T_{modSTC})\right) \tag{35}$$

This correction is done through the peak power temperature coefficient, $\alpha_{P_{max}}$, often provided in the datasheet of the photovoltaic modules, being T_{modSTC} the temperature of the photovoltaic cell at STC, namely 25°C.

The necessary parameters for the direct computation of the power output of a module in real conditions using equivalent circuit models are not readily available. Still, the only commonly available electrical characteristics from the manufacturers are the maximum power (P_{max}), current (I_{mp}) and voltage (V_{mp}) at maximum power, short-circuit current (I_{sc}) and open-circuit voltage (V_{oc}), all for standard test conditions (STC). The parameters needed for a given equivalent electric circuit model need to be computed from these values and then adjusted for the real conditions in the field, namely different conditions of incident solar irradiance and cell temperature.

The single diode and 5 parameters model (1d5p) as represented in Fig. A.1 and with I-V curve equation as given in Eq. (36) includes a current source which is caused by the photovoltaic effect and called photovoltaic current, I_{pv}, in parallel with a diode behaving as the p-n junction and a resistance, R_p, which accounts for the leakage current in the p-n junction and a series resistance, R_s, that represents the electric resistances of the silicon, of the electrodes and the contact between these materials. In this model, the five parameters were determined based on the method presented by Castro (Castro, 2018) in which expressions for the parameters I_{0STC} and I_{pvSTC} are obtained as a function of the remaining three parameters, which in turn are obtained from the equations at the three characteristic points in the I-V curve, thus resulting in the system of equations given by Eqs. (37) through (41).
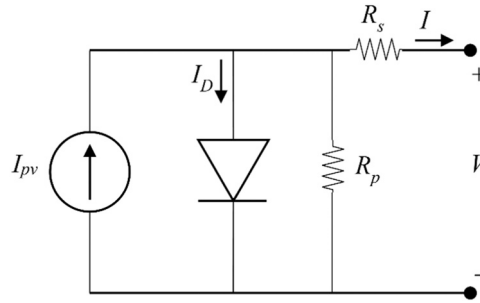
Fig. A.1. - Single diode and 5 parameters equivalent electric circuit.

$$I = I_{pv} - I_0 \left(e^{\frac{V+IR_s}{mV_T}} - 1 \right) - \frac{V+IR_s}{R_p} \tag{36}$$

$$I_{mpSTC} = I_{scSTC} - \frac{V_{mpSTC} + R_s I_{mpSTC} - R_s I_{scSTC}}{R_p} - \left(I_{scSTC} - \frac{V_{ocSTC} - R_s I_{scSTC}}{R_p} \right) e^{\frac{V_{mpSTC} + R_s I_{mpSTC} - V_{ocSTC}}{mV_{TSTC}}} \tag{37}$$

$$0 = I_{mpSTC} + \frac{-\frac{\left(R_p I_{scSTC} - V_{ocSTC} + R_s I_{scSTC} \right) e^{\frac{V_{mpSTC} + R_s I_{mpSTC} - V_{ocSTC}}{mV_{TSTC}}}}{mV_{TSTC}R_p} - \frac{1}{R_p}}{1 + \frac{R_s \left(R_p I_{scSTC} - V_{ocSTC} + R_s I_{scSTC} \right) e^{\frac{V_{mpSTC} + R_s I_{mpSTC} - V_{ocSTC}}{mV_{TSTC}}}}{mV_{TSTC}R_p} + \frac{R_s}{R_p}} \tag{38}$$

$$\frac{-\frac{\left(R_p I_{scSTC} - V_{ocSTC} + R_s I_{scSTC} \right) e^{\frac{R_s I_{scSTC} - V_{ocSTC}}{mV_{TSTC}}}}{mV_{TSTC}R_p} - \frac{1}{R_p}}{1 + \frac{R_s \left(R_p I_{scSTC} - V_{ocSTC} + R_s I_{scSTC} \right) e^{\frac{R_s I_{scSTC} - V_{ocSTC}}{mV_{TSTC}}}}{mV_{TSTC}R_p} + \frac{R_s}{R_p}} = -\frac{1}{R_p} \tag{39}$$

$$I_{0STC} = \left(I_{scSTC} - \frac{V_{ocSTC} - R_s I_{scSTC}}{R_p} \right) e^{\frac{-V_{ocSTC}}{m_{STC}V_{TSTC}}} \tag{40}$$

$$I_{pvSTC} = I_{0STC} e^{\frac{V_{ocSTC}}{m_{STC}V_{TSTC}}} + \frac{V_{ocSTC}}{R_p} \tag{41}$$

The real conditions in the field must be considered, which is done through Eq. (42) to (47).

$$I_{sc} = I_{scSTC} \frac{S \times M}{GSTC} \left(1 + \alpha_{Isc}(T_{\text{mod}} - T_{\text{modSTC}}) \right) \tag{42}$$

$$V_{oc.g} = mV_{TSTC} \ln \left(\frac{\frac{S \times M}{GSTC} I_{pvSTC} R_p - V_{oc.g}}{I_{0STC} R_p} \right) \tag{43}$$

$$V_{oc} = V_{oc.g} \left(1 + \alpha_{Voc}(T_{\text{mod}} - T_{\text{modSTC}}) \right) \tag{44}$$

$$m = m_{STC} \tag{45}$$

$$I_0 = \left(I_{sc} - \frac{V_{oc} - R_s I_{sc}}{R_p} \right) e^{\frac{-V_{oc}}{mV_T}} \tag{46}$$

$$I_{pv} = I_0 e^{\frac{V_{oc}}{mV_T}} + \frac{V_{oc}}{R_p} \tag{47}$$

Finally, the power output is estimated through Eq. (48) and a system of non-linear equations, Eqs. (49) and (50), with initial values given by Eqs. (51) and (52).

$$P_e = V_{mp} \times I_{mp} \tag{48}$$

$$I_{mp} = I_{sc} - \frac{V_{mp} + R_s I_{mp} - R_s I_{sc}}{R_p} - \left(I_{sc} - \frac{V_{oc} - R_s I_{sc}}{R_p} \right) e^{\frac{V_{mp} + R_s I_{mp} - V_{oc}}{mV_T}} \tag{49}$$

$$\frac{-\frac{\left(R_p I_{sc} - V_{oc} + R_s I_{sc} \right) e^{\frac{V_{mp} + R_s I_{mp} - V_{oc}}{mV_T}}}{mV_T R_p} - \frac{1}{R_p}}{1 + \frac{R_s \left(R_p I_{sc} - V_{oc} + R_s I_{sc} \right) e^{\frac{V_{mp} + R_s I_{mp} - V_{oc}}{mV_{TSTC}}}}{mV_T R_p} + \frac{R_s}{R_p}} = -\frac{I_{mp}}{V_{mp}} \tag{50}$$

$$I_{mp}(0) = I_{mpSTC}(1 + \alpha_{Isc}(T_{mod} - T_{modSTC}))$$ (51)

$$V_{mp}(0) = V_{mpSTC}(1 + \alpha_{Voc}(T_{mod} - T_{modSTC}))$$ (52)

The recently published international standard IEC 60891 ED3 (IEC, 2021IEC, 2021), specifically the procedure 4.4.4, was used in this work as an empirical model based on measurements for comparison and as a reference for this type of modeling approach. This model requires the current and voltage values at the three characteristic points of the I-V curve for four different conditions of incident irradiance and temperature.

This dataset was obtained for the four systems considered in this work through indoor measurements in the lab for various combinations of irradiance at normal incidence and cell temperature, namely (1000 W/m^2, 25 ℃), (1000 W/m^2, 60 ℃), (200 W/m^2, 25 ℃) and (200 W/m^2, 60 ℃) by means of a solar simulator and a temperature chamber at AIST (Ustun et al., 2019). The solar simulator is comprised of six xenon lamps with elliptical mirrors and ultraviolet, AM1.5 G and iron net dark filters with an output range of 100–1300 W/m^2 while the temperature chamber has a range of 15 ℃ to 65 ℃ (Ustun et al., 2019).

The current and voltage for maximum power in real conditions is then obtained through bi-linear interpolation thus allowing for the estimation of the power output.

The electric models presented were used to estimate the power output of the four different photovoltaic systems using the measured *GTI*, *DNI* and module temperature data, thus generating 10-minute power output values for each electric model. Results were compared to the power output measurements and with each other as shown in Table A.1. The same statistical indicators for each system/technology are presented separately in Table A.2. All models tend to show an overestimation of the power output which can result in part from the fact that the temperature used as input to these models is the one measured at the back of the photovoltaic modules and not the photovoltaic cell temperature. It might be the case, as it often is, that the temperature measured this way is lower than the actual temperature of the cell and consequently the power estimated will be higher than the actual power output of the photovoltaic module.

The IEC model was shown to have better results which was expected since it is based on measurements of the specific systems assessed in this work. The following model is the simple estimate with temperature correction which, although not as detailed, achieved in this case better results than the single diode and 5 parameters model, especially in terms of RMSE. Both of these models perform slightly better for systems 2 and 3 (HIT and poly-crystalline technologies, see Table A.2).

Table A.1
Statistical metrics of the electric model results.

Model	R^2	MBE (W)	rMBE (%)	RMSE (W)	rRMSE (%)	GPI
IEC	0.994	−3.6	−0.6	59.0	9.2	0.511
SET	0.994	13.7	2.1	57.4	8.9	0.108
1d5p	0.987	16.3	2.5	84.8	13.2	−2.020

Table A.2
– Statistical indicators of the results of electric models using measured temperature for each system.

Model	System	R^2	MBE (W)	rMBE (%)	RMSE (W)	rRMSE (%)
SET	1	0.988	26.2	4.0	61.8	9.3
	2	0.992	4.0	0.6	52.5	7.9
	3	0.991	2.3	0.3	55.4	8.4
	4	0.989	22.4	3.4	59.4	9.0
1d5p	1	0.970	36.6	5.5	99.1	15.0
	2	0.982	4.6	0.7	77.6	11.7
	3	0.981	5.1	0.8	78.9	12.0
	4	0.980	18.8	2.8	81.7	12.4
IEC	1	0.989	18.5	2.8	59.4	9.0
	2	0.987	−32.8	−5.0	66.3	10.0
	3	0.991	−0.9	−0.1	55.6	8.4
	4	0.991	0.9	0.1	54.0	8.2

Appendix B. - Temperature model results for each photovoltaic system

Table B.1
- Statistical indicators of the results of thermal models when compared to the measured temperature for each system.

Model	System	R^2	MBE (°C)	rMBE (%)	RMSE (°C)	rRMSE (%)
Modified Chenni	1	0.857	−2.9	−11.3	4.6	18.0
	2	0.885	−2.1	−8.2	4.2	16.9
	3	0.828	−3.6	−13.5	5.1	19.4
	4	0.857	−2.9	−11.3	4.6	18.0
Mattei	1	0.951	−0.3	−1.0	2.7	10.5
	2	0.952	0.2	0.8	2.7	10.9
	3	0.952	−0.9	−3.3	2.7	10.2
	4	0.949	−0.5	−1.9	2.8	10.8

Table B.1 (*continued*)

Model	System	R^2	MBE (°C)	rMBE (%)	RMSE (°C)	rRMSE (%)
Kurtz (Sandia1)	1	0.909	2.0	7.7	3.7	14.3
	2	0.896	2.8	11.4	4.0	16.1
	3	0.935	1.3	5.0	3.1	11.9
	4	0.909	2.0	7.7	3.7	14.3
Sandia3	1	0.947	0.9	3.4	2.8	11.0
	2	0.941	1.7	7.0	3.0	12.1
	3	0.959	0.2	0.8	2.5	9.4
	4	0.947	0.9	3.4	2.8	11.0
Faiman	1	0.939	1.6	6.2	3.0	11.7
	2	0.923	2.5	9.9	3.4	13.8
	3	0.958	0.9	3.5	2.5	9.5
	4	0.939	1.6	6.2	3.0	11.7
JIS1	1	0.933	0.8	2.9	3.2	12.3
	2	0.929	1.6	6.5	3.3	13.2
	3	0.948	0.1	0.4	2.8	10.7
	4	0.933	0.8	2.9	3.2	12.3
Migan	1	0.951	1.1	4.4	2.7	10.5
	2	0.939	2.0	8.0	3.1	12.3
	3	0.965	0.5	1.8	2.3	8.7
	4	0.951	1.1	4.4	2.7	10.5
Dynamic + SET	1	0.907	−0.8	−2.9	3.7	14.4
	2	0.935	−0.6	−2.3	3.2	12.6
	3	0.909	−1.4	−5.1	3.7	13.9
	4	0.915	−1.2	−4.8	3.6	13.8
Dynamic + 1d5p	1	0.902	−0.2	−0.8	3.9	14.8
	2	0.932	0.0	0.0	3.3	12.9
	3	0.909	−0.8	−2.8	3.7	13.9
	4	0.915	−0.6	−2.5	3.6	13.7

Table B.2

Statistical indicators of SET model output coupled with each thermal model for each system.

Model	System	R^2	MBE (W)	rMBE (%)	RMSE (W)	rRMSE (%)
Measured temperature	1	0.988	26.2	4.0	61.8	9.3
	2	0.992	4.0	0.6	52.5	7.9
	3	0.991	2.3	0.3	55.4	8.4
	4	0.989	22.4	3.4	59.4	9.0
Modified Chenni	1	0.982	41.6	6.3	76.6	11.6
	2	0.991	12.5	1.9	55.9	8.5
	3	0.989	20.3	3.1	60.4	9.2
	4	0.984	36.0	5.4	71.8	10.9
Mattei	1	0.989	28.1	4.2	61.3	9.3
	2	0.992	5.4	0.8	52.8	8.0
	3	0.991	6.5	1.0	53.4	8.1
	4	0.989	25.2	3.8	60.1	9.1
Kurtz (Sandia1)	1	0.991	15.3	2.3	54.6	8.3
	2	0.992	−4.0	−0.6	52.9	8.0
	3	0.990	−5.7	−0.9	56.8	8.6
	4	0.991	12.8	1.9	53.7	8.1
Sandia3	1	0.990	21.7	3.3	57.2	8.6
	2	0.992	0.0	0.0	52.3	7.9
	3	0.991	0.7	0.1	54.1	8.2
	4	0.991	18.5	2.8	55.8	8.4
Faiman	1	0.990	18.6	2.8	57.0	8.6
	2	0.992	−2.0	−0.3	52.7	8.0
	3	0.991	−2.5	−0.4	55.9	8.5
	4	0.991	15.7	2.4	55.5	8.4
JIS1	1	0.990	18.2	2.8	56.8	8.6
	2	0.992	−2.2	−0.3	52.8	8.0
	3	0.990	−2.8	−0.4	56.9	8.6
	4	0.991	15.4	2.3	55.3	8.4
Migan	1	0.990	20.9	3.2	57.6	8.7
	2	0.992	−0.5	−0.1	52.4	7.9
	3	0.991	−0.2	0.0	54.8	8.3
	4	0.991	17.7	2.7	56.1	8.5
Dynamic	1	0.990	22.4	3.4	56.2	8.5
	2	0.992	2.9	0.4	51.5	7.8
	3	0.991	0.7	0.1	54.1	8.2
	4	0.991	21.9	3.3	55.9	8.4

Table B.3
Statistical indicators of single diode and 5 parameters model output coupled with each thermal model for each system.

Model	System	R^2	MBE (W)	rMBE (%)	RMSE (W)	rRMSE (%)
	1	0.970	36.6	5.5	99.1	15.0
Measured	2	0.982	4.6	0.7	77.6	11.7
temperature	3	0.981	5.1	0.8	78.9	12.0
	4	0.980	18.8	2.8	81.7	12.4
	1	0.970	36.7	5.5	99.8	15.1
Modified	2	0.982	3.6	0.5	77.3	11.7
Chenni	3	0.980	6.5	1.0	81.1	12.3
	4	0.978	21.8	3.3	86.2	13.0
	1	0.970	36.8	5.6	99.5	15.0
Mattei	2	0.982	4.7	0.7	77.6	11.7
	3	0.981	5.7	0.9	79.6	12.1
	4	0.979	19.7	3.0	83.1	12.6
	1	0.971	36.5	5.5	98.4	14.9
Kurtz	2	0.982	5.5	0.8	77.6	11.7
(Sandia1)	3	0.982	4.4	0.7	77.9	11.8
	4	0.981	16.6	2.5	78.8	11.9
	1	0.970	36.7	5.6	99.0	15.0
Sandia3	2	0.982	5.2	0.8	77.6	11.7
	3	0.981	5.1	0.8	78.8	11.9
	4	0.980	18.1	2.7	80.8	12.2
	1	0.971	36.6	5.5	98.6	14.9
Faiman	2	0.982	5.3	0.8	77.5	11.7
	3	0.981	4.7	0.7	78.3	11.9
	4	0.981	17.3	2.6	79.8	12.1
	1	0.971	36.4	5.5	98.4	14.9
JIS1	2	0.982	5.2	0.8	77.6	11.7
	3	0.982	4.5	0.7	77.9	11.8
	4	0.981	17.0	2.6	79.2	12.0
	1	0.971	36.7	5.5	98.9	15.0
Migan	2	0.982	5.2	0.8	77.6	11.7
	3	0.981	5.0	0.8	78.6	11.9
	4	0.980	17.8	2.7	80.6	12.2
	1	0.971	36.5	5.5	98.8	14.9
Dynamic	2	0.982	5.0	0.8	77.8	11.8
	3	0.982	4.7	0.7	78.2	11.9
	4	0.981	18.0	2.7	80.3	12.1

References

Abbassi, R., Abbassi, A., Jemli, M., Chebbi, S., 2018. Identification of unknown parameters of solar cell models: a comprehensive overview of available approaches. Renew. Sustain. Energy Rev. https://doi.org/10.1016/j.rser.2018.03.011.

Bevilacqua, P., Perrella, S., Bruno, R., Arcuri, N., 2021. An accurate thermal model for the PV electric generation prediction: long-term validation in different climatic conditions. Renew. Energy 163, 1092–1112. https://doi.org/10.1016/j.renene.2020.07.115.

Castro, R., 2018. Data-driven PV modules modelling: comparison between equivalent electric circuit and artificial intelligence based models. Sustain. Energy Technol. Assess. 30, 230–238. https://doi.org/10.1016/J.SETA.2018.10.011.

Chenni, R., Makhlouf, M., Kerbache, T., Bouzid, A., 2007. A detailed modeling method for photovoltaic cells. Energy 32, 1724–1730. https://doi.org/10.1016/J.ENERGY.2006.12.006.

Chin, V.J., Salam, Z., Ishaque, K., 2015. Cell modelling and model parameters estimation techniques for photovoltaic simulator application: a review. Appl. Energy 154, 500–519. https://doi.org/10.1016/j.apenergy.2015.05.035.

Coskun, C., Toygar, U., Sarpdag, O., Oktay, Z., 2017. Sensitivity analysis of implicit correlations for photovoltaic module temperature: a review. J. Clean. Prod. 164, 1474–1485. https://doi.org/10.1016/j.jclepro.2017.07.080.

De Soto, W., Klein, S.A., Beckman, W.A., 2006. Improvement and validation of a model for photovoltaic array performance. Sol. Energy 80, 78–88. https://doi.org/10.1016/j.solener.2005.06.010.

Dormand, J.R., Prince, P.J., 1986. A reconsideration of some embedded Runge-Kutta formulae. J. Comput. Appl. Math. 15, 203–211. https://doi.org/10.1016/0377-0427(86)90027-0.

Duffie, J.A., Beckman, W.A., 2013. Solar Engineering of Thermal Processes 1–885.

Evans, D.L., Florschuetz, L.W., 1977. Cost studies on terrestrial photovoltaic power systems with sunlight concentration. Sol. Energy 19, 255–262. https://doi.org/10.1016/0038-092X(77)90068-8.

Fahim, S.R., Hasanien, H.M., Turky, R.A., Aleem, S.H.E.A., Ćalasan, M., 2022. A comprehensive review of photovoltaic modules models and algorithms used in parameter extraction. Energ. (Basel) 15, 1–56. https://doi.org/10.3390/en15238941.

Faiman, D., 2008. Assessing the outdoor operating temperature of photovoltaic modules. Prog. Photovolt.: Res. Appl. 16, 307–315. https://doi.org/10.1002/pip.813.

Fujii, T., Imura, H., 1972. Natural-convection heat transfer from a plate with arbitrary inclination. Int J. Heat. Mass Transf. 15, 755–767. https://doi.org/10.1016/0017-9310(72)90118-4.

Gholami, A., Ameri, M., Zandi, M., Gavagsaz Ghoachani, R., Kazem, H.A., 2022b. Predicting solar photovoltaic electrical output under variable environmental conditions: Modified semi-empirical correlations for dust. Energy Sustain. Dev. 71, 389–405. https://doi.org/10.1016/J.ESD.2022.10.012.

Gholami, A., Ameri, M., Zandi, M., Gavagsaz Ghoachani, R., 2022a. Electrical, thermal and optical modeling of photovoltaic systems: step-by-step guide and comparative review study. Sustain. Energy Technol. Assess. 49, 101711 https://doi.org/10.1016/j.seta.2021.101711.

Gholami, A., Ameri, M., Zandi, M., Gavagsaz Ghoachani, R., Jafarzadegan Gerashi, S., Kazem, H.A., Al-Waeli, A.H.A., 2023. Impact of harsh weather conditions on solar photovoltaic cell temperature: experimental analysis and thermal-optical modeling. Sol. Energy 252, 176–194. https://doi.org/10.1016/J.SOLENER.2023.01.039.

Gu, W., Ma, T., Shen, L., Li, M., Zhang, Y., Zhang, W., 2019. Coupled electrical-thermal modelling of photovoltaic modules under dynamic conditions. Energy 188, 116043. https://doi.org/10.1016/j.energy.2019.116043.

Hasan, M.A., Parida, S.K., 2016. An overview of solar photovoltaic panel modeling based on analytical and experimental viewpoint. Renew. Sustain. Energy Rev. 60, 75–83. https://doi.org/10.1016/j.rser.2016.01.087.

IEC, 2021. IEC 60891:2021 ED3 Photovoltaic devices - Procedures for temperature and irradiance corrections to measured I-V characteristics.

Japanese Industrial Standard - Japanese Standards Association, 2005. Estimation method of generating electric energy by PV power system. JIS C. 8907, 2005.

Kalogirou, S.A., 2009. Solar Energy Engineering: processes and systems. Academic Press Inc.

Kaplani, E., Kaplanis, S., 2014. Thermal modelling and experimental assessment of the dependence of PV module temperature on wind velocity and direction, module orientation and inclination. Sol. Energy 107, 443–460. https://doi.org/10.1016/j.solener.2014.05.037.

Kaplanis, S., Kaplani, E., 2019. A new dynamic model to predict transient and steady state pv temperatures taking into account the environmental conditions. Energ. (Basel) 12. https://doi.org/10.3390/en12010002.

Kazem, H.A., Chaichan, M.T., Al-Waeli, A.H.A., Al-Badi, R., Fayad, M.A., Gholami, A., 2022. Dust impact on photovoltaic/thermal system in harsh weather conditions. Sol. Energy 245, 308–321. https://doi.org/10.1016/J.SOLENER.2022.09.012.

Li, F., Wu, W., 2022. Coupled electrical-thermal performance estimation of photovoltaic devices: A transient multiphysics framework with robust parameter extraction and 3-D thermal analysis. Appl. Energy 319, 119249. https://doi.org/10.1016/j.apenergy.2022.119249.

Luketa-Hanlin, A., Stein, J.S., 2012. Improvement and validation of a transient model to predict photovoltaic module temperature, in: World Renewable Energy Forum.

Ma, T., Yang, H., Lu, L., 2014. Solar photovoltaic system modeling and performance prediction. Renew. Sustain. Energy Rev. 36, 304–315. https://doi.org/10.1016/J.RSER.2014.04.057.

Mattei, M., Notton, G., Cristofari, C., Muselli, M., Poggi, P., 2006. Calculation of the polycrystalline PV module temperature using a simple method of energy balance. Renew. Energy 31, 553–567. https://doi.org/10.1016/J.RENENE.2005.03.010.

Mermoud, A., Lejeune, T., 2010. Performance Assessment of a Simulation Model for PV Modules of Any Available Technology, in: Proceedings of the 25th European Photovoltaic Solar Energy Conference.

Migan, G.-A., 2013. Project Report 2013 MVK160 Heat and Mass Transfer Study of the operating temperature of a PV module.

Pereira, S., Canhoto, P., Salgado, R., 2023. Development and assessment of artificial neural network models for direct normal solar irradiance forecasting using operational numerical weather prediction data. Energy AI, 100314. https://doi.org/10.1016/j.egyai.2023.100314.

Perovic, B., Klimenta, D., Jevtic, M., Milovanovic, M., 2019. A transient thermal model for flat-plate photovoltaic systems and its experimental validation. Elektron. Ir. Elektro 25, 40–46. https://doi.org/10.5755/j01.eie.25.2.23203.

Reiter, C.N., Trinkl, C., Zörner, W., Hanby, V.I., 2015. A dynamic multinode model for component-oriented thermal analysis of flat-plate solar collectors. J. Sol. Energy 2015, 1–16. https://doi.org/10.1155/2015/280694.

Roberts, J.J., Mendiburu Zevallos, A.A., Cassula, A.M., 2017. Assessment of photovoltaic performance models for system simulation. Renew. Sustain. Energy Rev. 72, 1104–1123. https://doi.org/10.1016/J.RSER.2016.10.022.

Sandia National Laboratories, n.d. Sandia Module Temperature Model [WWW Document]. URL ⟨https://pvpmc.sandia.gov/modeling-steps/2-dc-module-iv/module-temperature/sandia-module-temperature-model/⟩ (accessed 1.24.23).

Sartori, E., 2006. Convection coefficient equations for forced air flow over flat surfaces. Sol. Energy 80, 1063–1071. https://doi.org/10.1016/J.SOLENER.2005.11.001.

Skoplaki, E., Palyvos, J.A., 2009. Operating temperature of photovoltaic modules: a survey of pertinent correlations. Renew. Energy 34, 23–29. https://doi.org/10.1016/j.renene.2008.04.009.

Swinbank, W.C., 1963. Long-wave radiation from clear skies. Q. J. R. Meteorol. Soc. 89, 339–348. https://doi.org/10.1002/qj.49708938105.

Tina, G., 2010. A Coupled Electrical and Thermal Model for Photovoltaic Modules. J. Sol. Energy Eng. 132 https://doi.org/10.1115/1.4001149.

Torres-Lobera, D., Valkealahti, S., 2014. Inclusive dynamic thermal and electric simulation model of solar PV systems under varying atmospheric conditions. Sol. Energy 105, 632–647. https://doi.org/10.1016/j.solener.2014.04.018.

Tuncel, B., Ozden, T., Balog, R.S., Akinoglu, B.G., 2020. Dynamic thermal modelling of PV performance and effect of heat capacity on the module temperature. Case Stud. Therm. Eng. 22, 100754 https://doi.org/10.1016/j.csite.2020.100754.

Tuomiranta, A., Marpu, P., Munawwar, S., Ghedira, H., 2014. Validation of thermal models for photovoltaic cells under hot desert climates. Energy Procedia 57, 136–143. https://doi.org/10.1016/j.egypro.2014.10.017.

Ustun, T.S., Nakamura, Y., Hashimoto, J., Otani, K., 2019. Performance analysis of PV panels based on different technologies after two years of outdoor exposure in Fukushima, Japan. Renew. Energy 136, 159–178. https://doi.org/10.1016/J.RENENE.2018.12.100.